Electronic Supplementary Material (ESI) for Journal of Materials Chemistry C.

Designing for dopability in semiconducting $AgInTe_2$: Supporting Information

Vanessa Meschke,[†] Lídia Carvalho Gomes,[‡] Jesse M. Adamczyk,[†] Kamil M. Ciesielski,[†] Caitlin M. Crawford,[†] Haley Vinton,[¶] Elif Ertekin,[‡] and Eric S. Toberer*,[†]

†*Department of Physics, Golden, CO 80401*

‡*Department of Mechanical Science and Engineering, Champaign, Illinois 61820*

¶*Department of Mathematics, Golden, CO 80401*

E-mail: etoberer@mines.edu

1 Experimental Determination of Phase Diagram

1.1 Region AI1: $AgInTe_2$, Ag, and Ag_3In

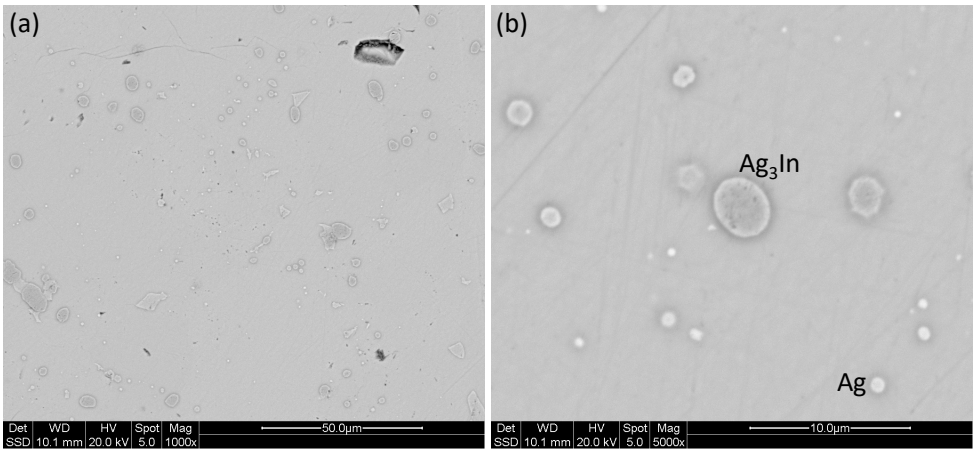

Figure S1 (a) 1000x and (b) 5000x magnification for a nominal stoichiometry of $Ag_{1.09}In_{0.98}Te_{1.93}$ showing dark regions of Ag_3In and light regions of elemental Ag in a matrix of $AgInTe_2$.

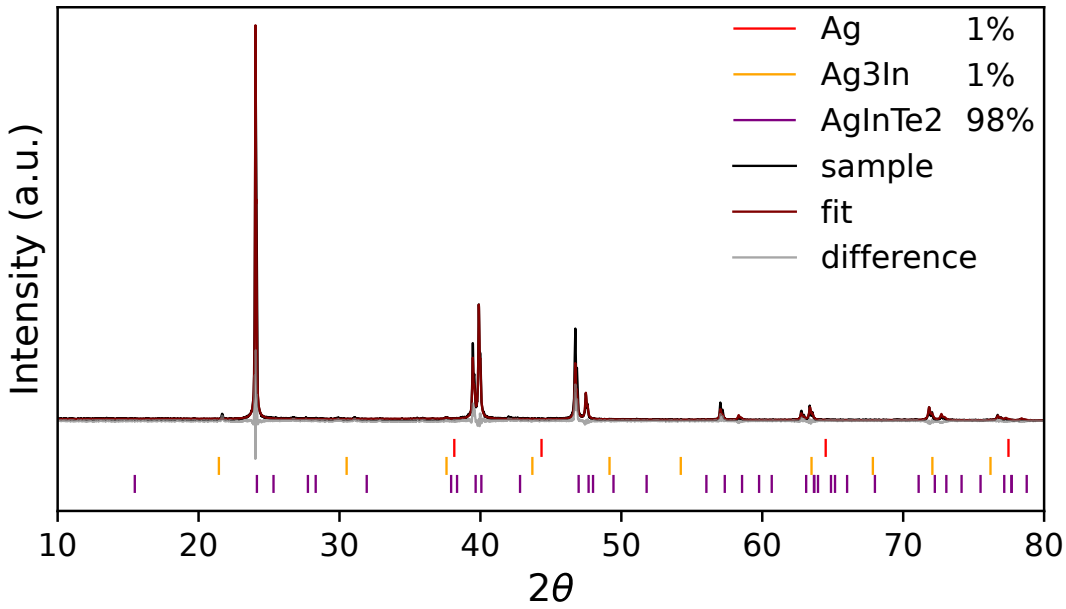

Figure S2 Powder XRD patterns for a nominal stoichiometry of $Ag_{1.09}In_{0.98}Te_{1.93}$ mostly showing the powder XRD pattern for $AgInTe_2$ with very slight impurity phases.

1.2 Region AI2: $AgInTe_2$, Ag_3In, and InTe

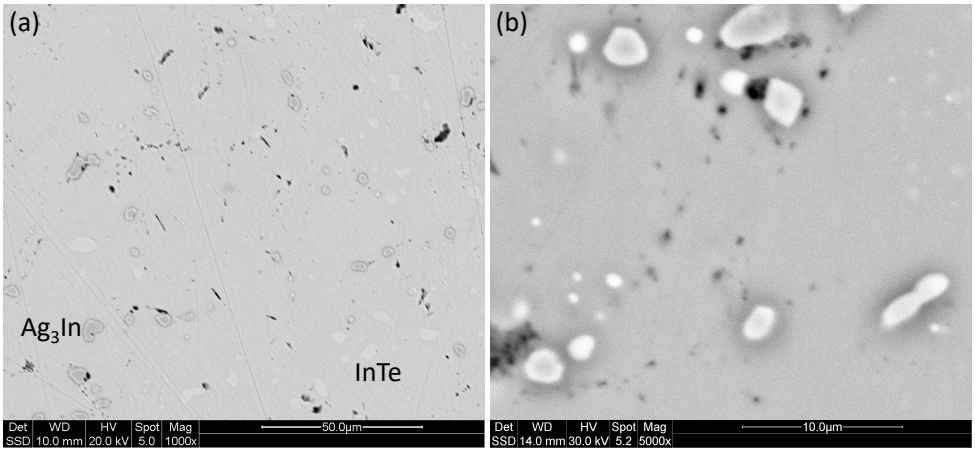

Figure S3 (a) 1000x and (b) 5000x magnification for a nominal stoichiometry of $AgInTe_{1.96}$ showing dark regions of Ag_3In and light regions of InTe in a matrix of $AgInTe_2$.

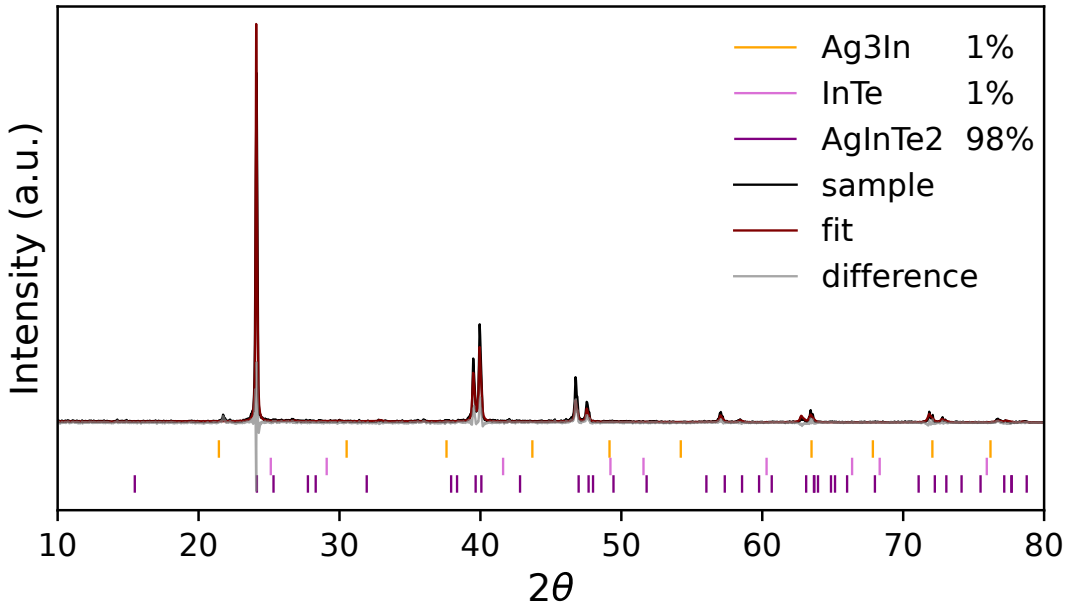

Figure S4 Powder XRD pattern for a nominal stoichiometry of $AgInTe_{1.96}$ mostly showing the powder XRD pattern for $AgInTe_2$ with very slight impurity phases.

1.3 Region IT1: $AgInTe_2$, $AgIn_5Te_8$, and InTe

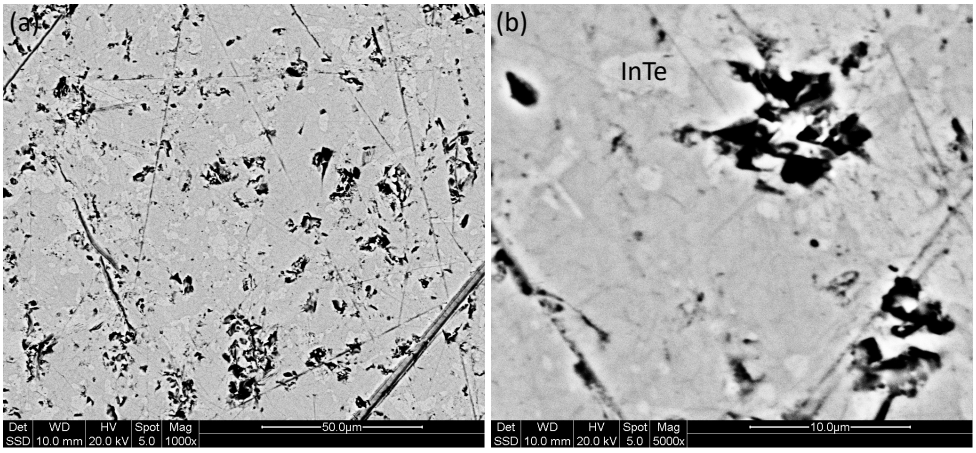

Figure S5 (a) 1000x and (b) 5000x magnification for a nominal stoichiometry of $Ag_{0.6}In_{1.32}Te_{2.08}$ showing lighter regions of InTe in a matrix composed of 20% Ag, 30% In, and 50% Te, consistent with a solid solution made of $AgInTe_2$ and $AgIn_5Te_8$.

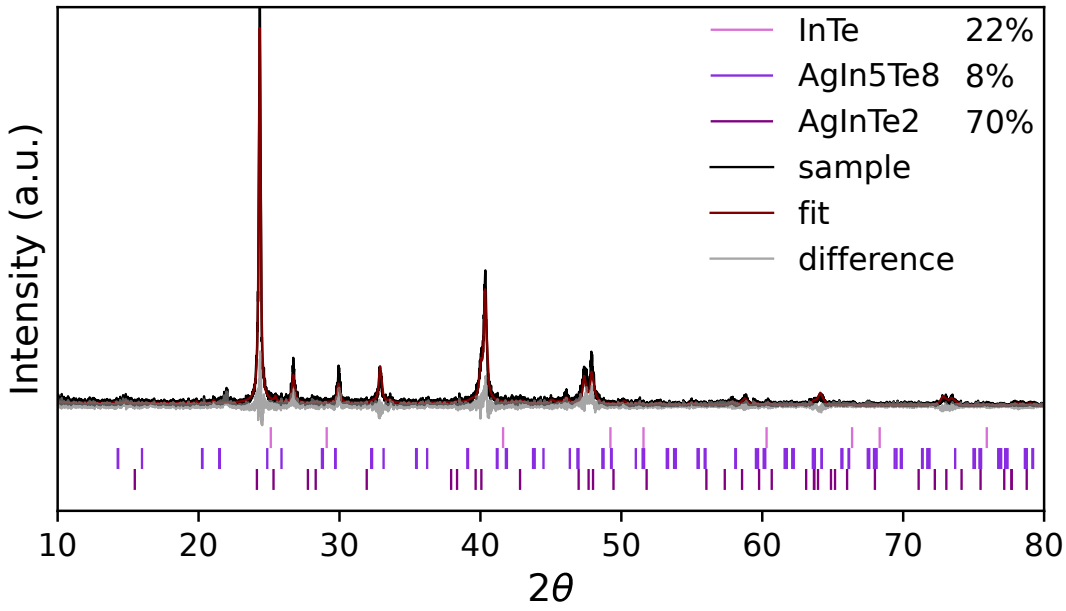

Figure S6 Powder XRD pattern for a nominal stoichiometry of $Ag_{0.6}In_{1.32}Te_{2.08}$ largely showing $AgInTe_2$ and InTe.

1.4 Region IT2: $AgInTe_2$, $AgIn_5Te_8$, and Te

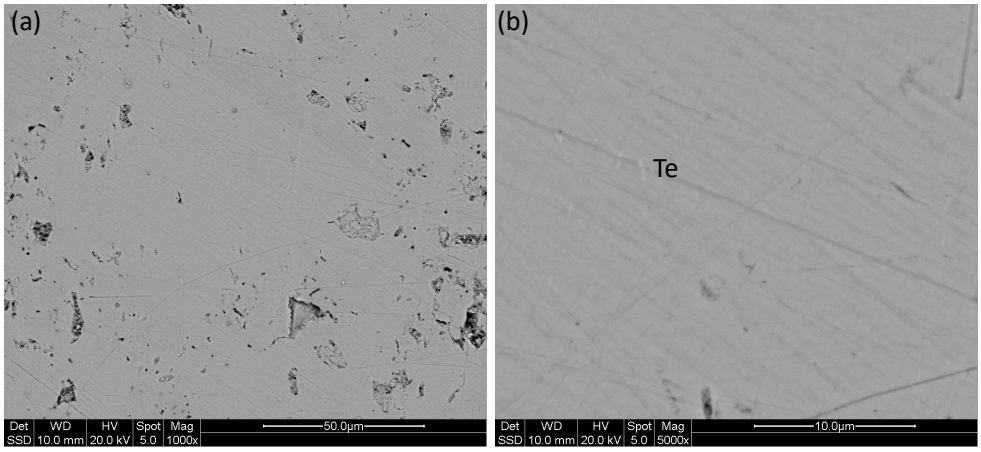

Figure S7 (a) 1000x and (b) 5000x magnification for a nominal stoichiometry of $Ag_{0.98}InTe_2$ showing a matrix composed of 20% Ag, 30% In, and 50% Te, consistent with a solid solution made of $AgInTe_2$ and $AgIn_5Te_8$ with some faint light spots of elemental Te.

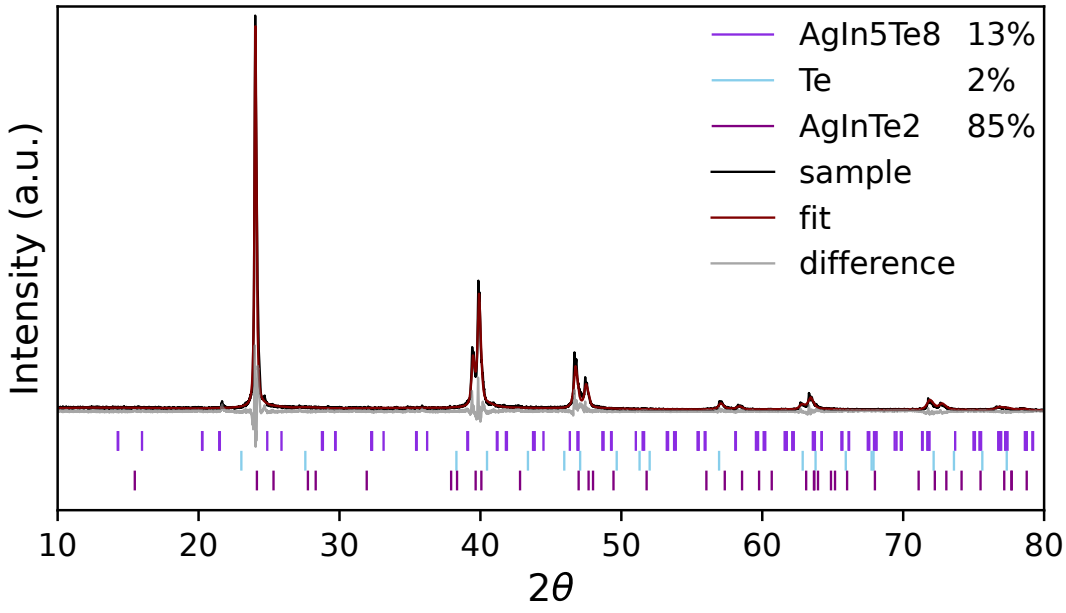

Figure S8 Powder XRD pattern for a nominal stoichiometry of $Ag_{0.98}InTe_2$ largely showing $AgInTe_2$.

1.5 Region AT1: $AgInTe_2$, Te, and AgTe

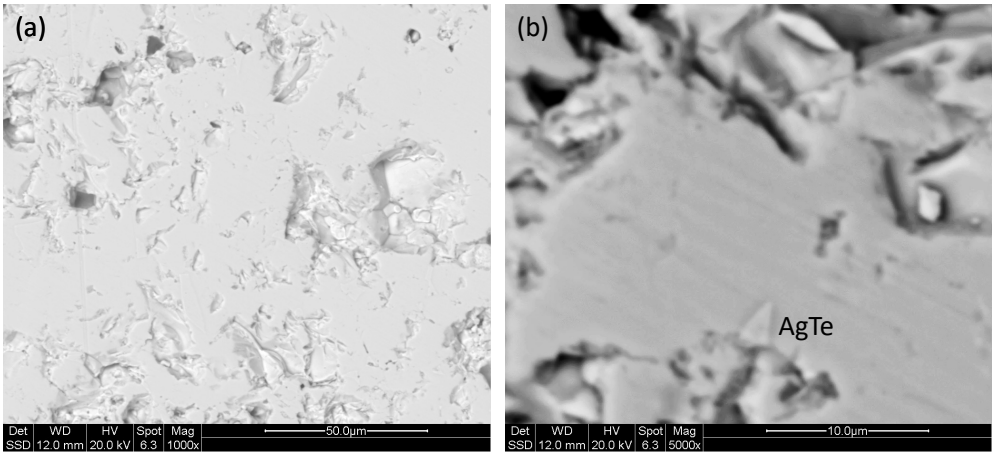

Figure S9 (a) 1000x and (b) 5000x magnification for a nominal stoichiometry of $Ag_{1.24}In_{0.4}Te_{2.36}$ showing a small region of AgTe in a matrix of $AgInTe_2$.

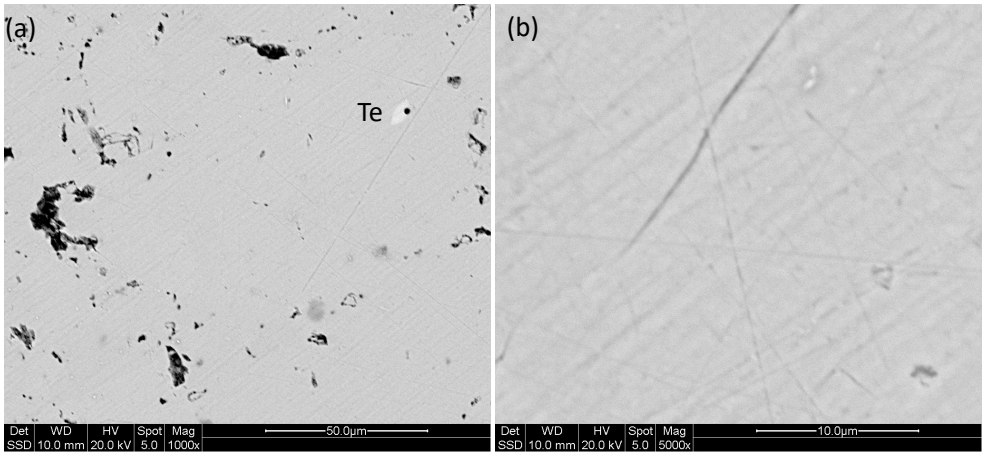

Figure S10 (a) 1000x and (b) 5000x magnification for a nominal stoichiometry of $AgIn_{0.98}Te_2$ showing a small region of Te in a matrix of $AgInTe_2$.

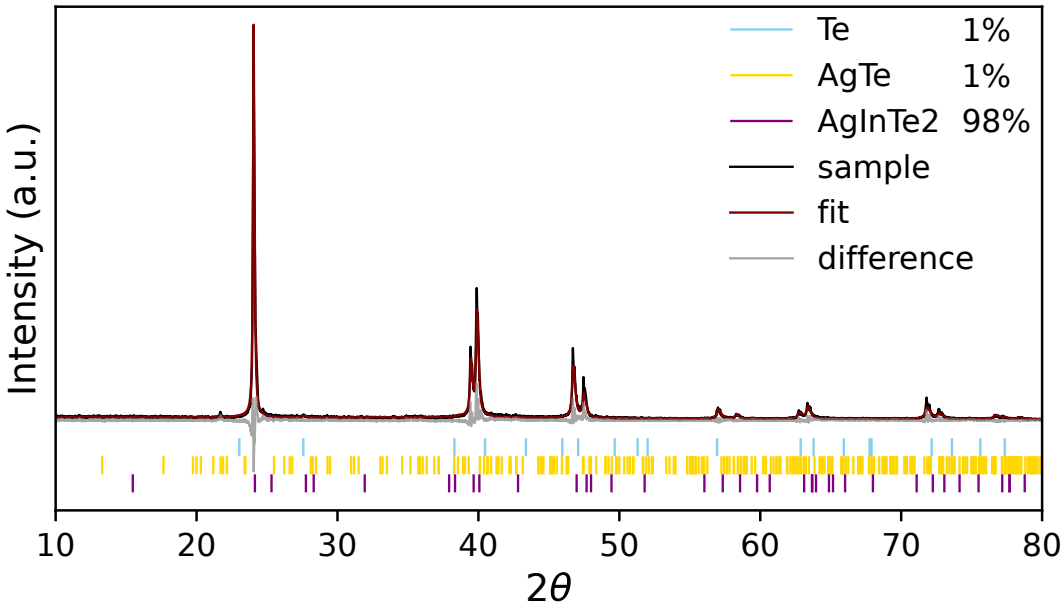

Figure S11 Powder XRD pattern for a nominal stoichiometry of $AgIn_{0.98}Te_2$ largely showing $AgInTe_2$.

1.6 Region AT2: $AgInTe_2$, Ag_2Te, and AgTe

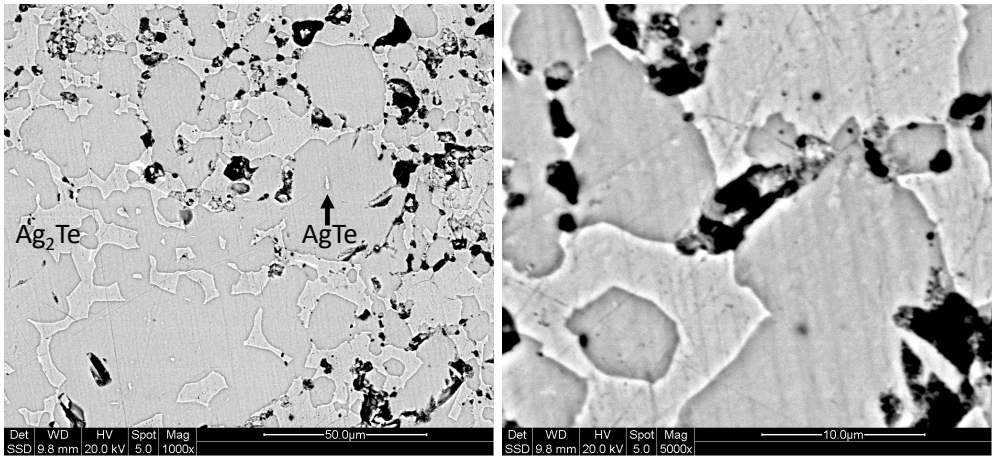

Figure S12 (a) 1000x and (b) 5000x magnification for a nominal stoichiometry of $Ag_{1.6}In_{0.6}Te_{1.8}$ showing small, very bright regions of AgTe and larger, slightly darker regions of Ag_2Te in a matrix of $AgInTe_2$.

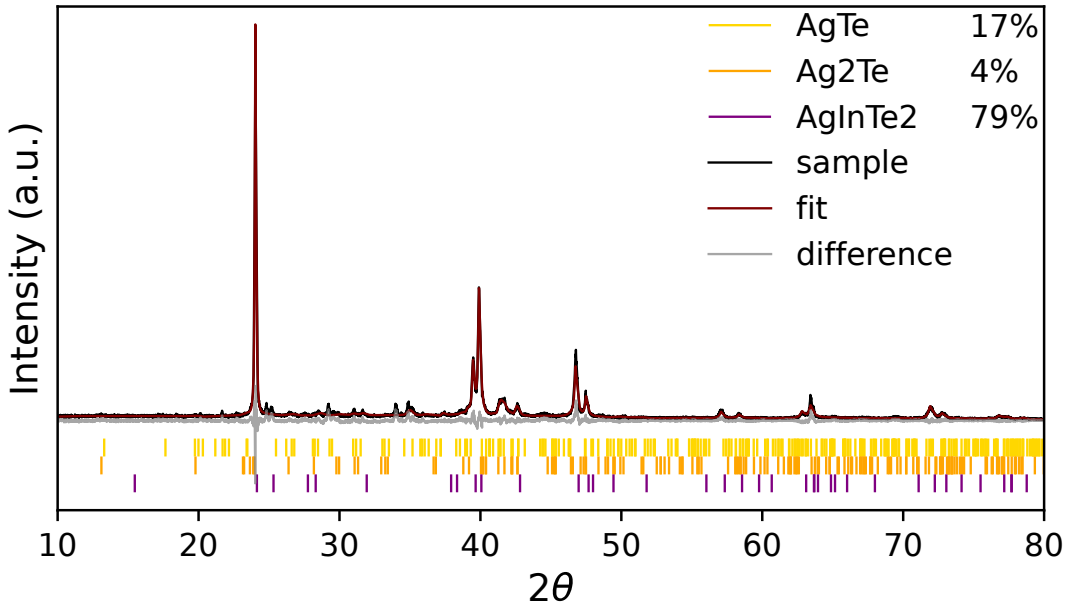

Figure S13 Powder XRD pattern for a nominal stoichiometry of $Ag_{1.6}In_{0.6}Te_{1.8}$ largely showing $AgInTe_2$.

1.7 Region AT3: $AgInTe_2$, Ag_2Te, and Ag

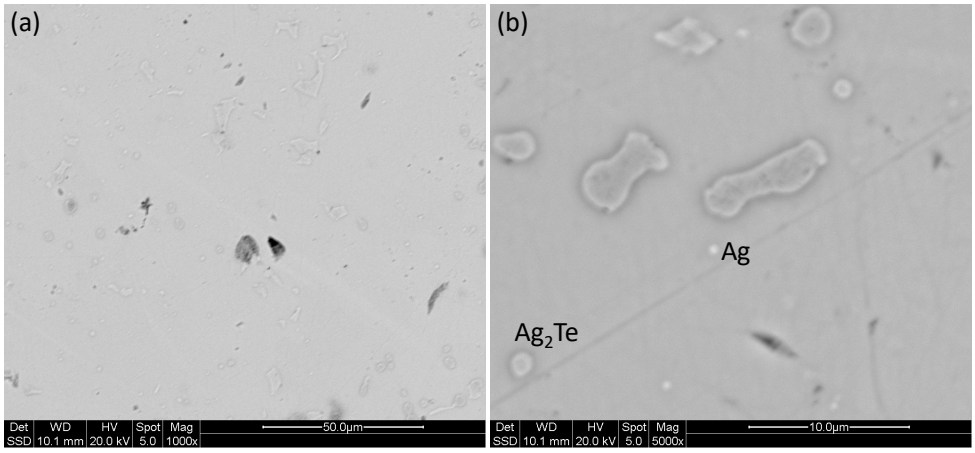

Figure S14 (a) 1000x and (b) 5000x magnification for a nominal stoichiometry of $Ag_{1.11}In_{0.95}Te_{1.94}$ showing elemental Ag as the brightest, small dots and AgTe as the larger, slightly darker regions in a matrix of $AgInTe_2$.

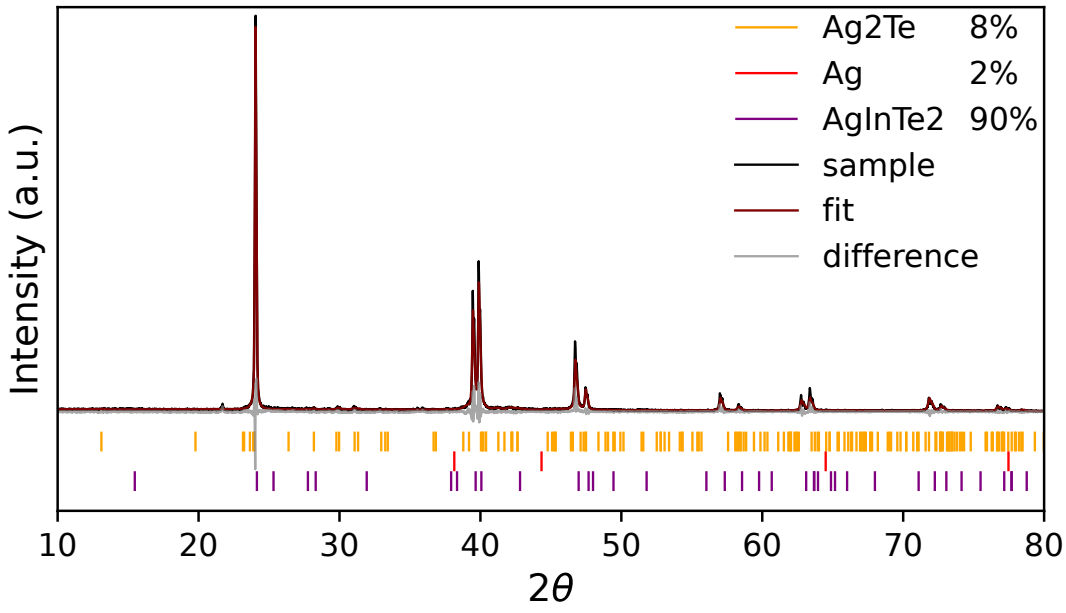

Figure S15 Powder XRD pattern for a nominal stoichiometry of $Ag_{1.11}In_{0.95}Te_{1.94}$ largely showing $AgInTe_2$.

2 Structural Analysis of Doped Samples

2.1 AI2 + Ge

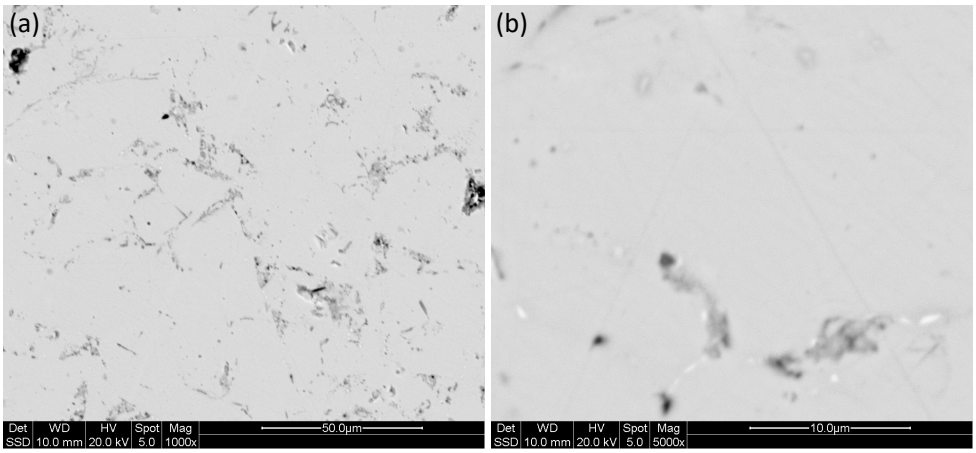

Figure S16 (a) 1000x and (b) 5000x magnification for a nominal stoichiometry of $AgInTe_{1.96}Ge_{0.02}$ showing a matrix of $AgInTe_2$ with up to 6% Ge incorporated. Brighter spots have a composition of 22% Ag, 28% In, 33% Te, and 17% Ge according to EDS.

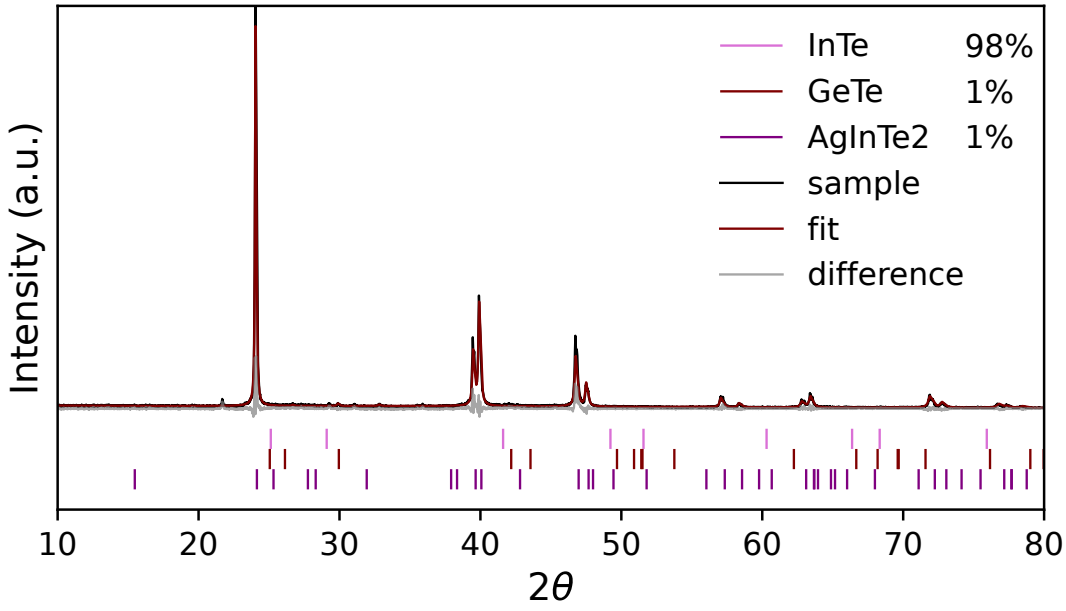

Figure S17 Powder XRD pattern for a nominal stoichiometry of $AgInTe_{1.96}Ge_{0.02}$ largely showing $AgInTe_2$.

2.2 AI2 + Zn

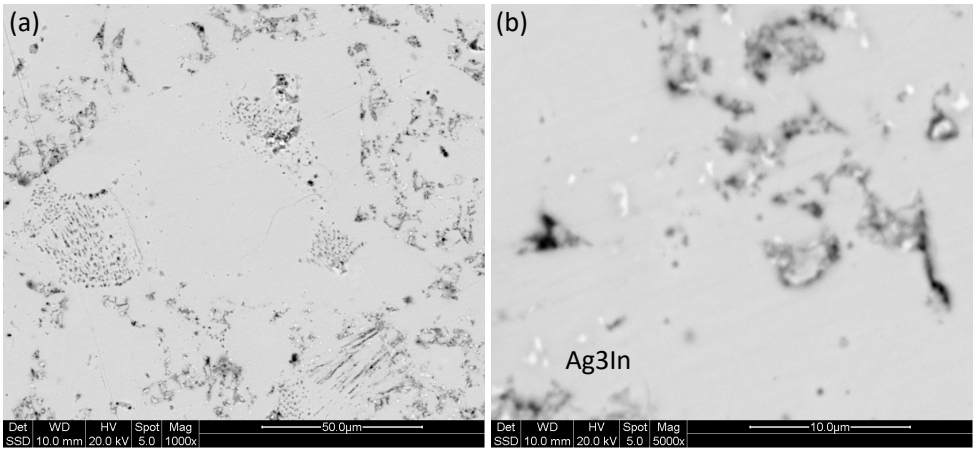

Figure S18 (a) 1000x and (b) 5000x magnification for a nominal stoichiometry of $AgInTe_{1.96}Zn_{0.02}$ showing Ag_3In as the brighter dots in a matrix of slightly silver-deficient $AgInTe_2$ with approximately 3% Zn incorporated.

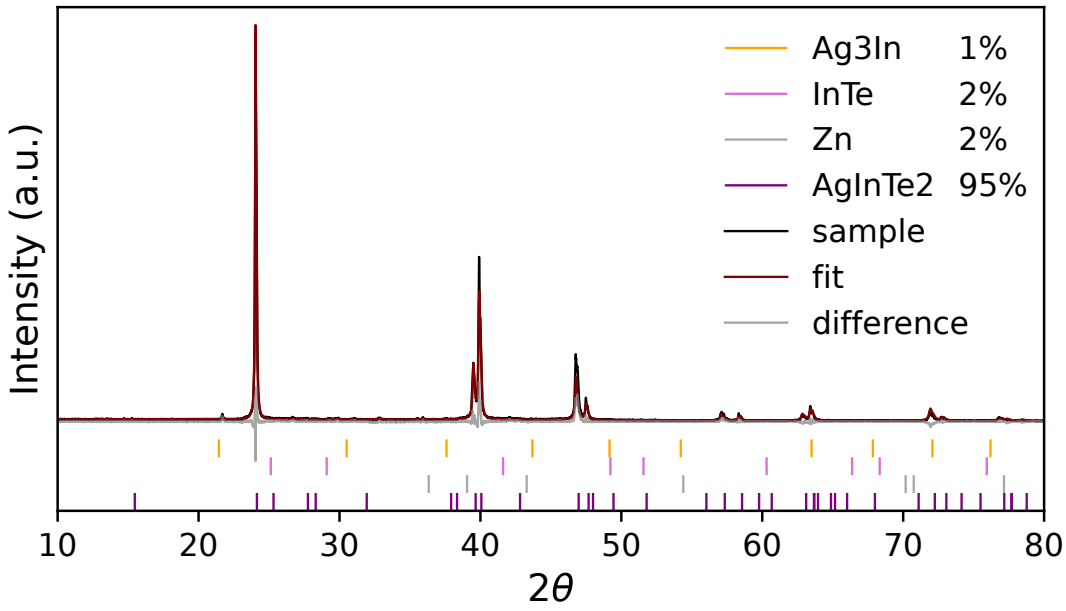

Figure S19 Powder XRD pattern for a nominal stoichiometry of $AgInTe_{1.96}Zn_{0.02}$ largely showing $AgInTe_2$.

2.3 IT2 + Ge

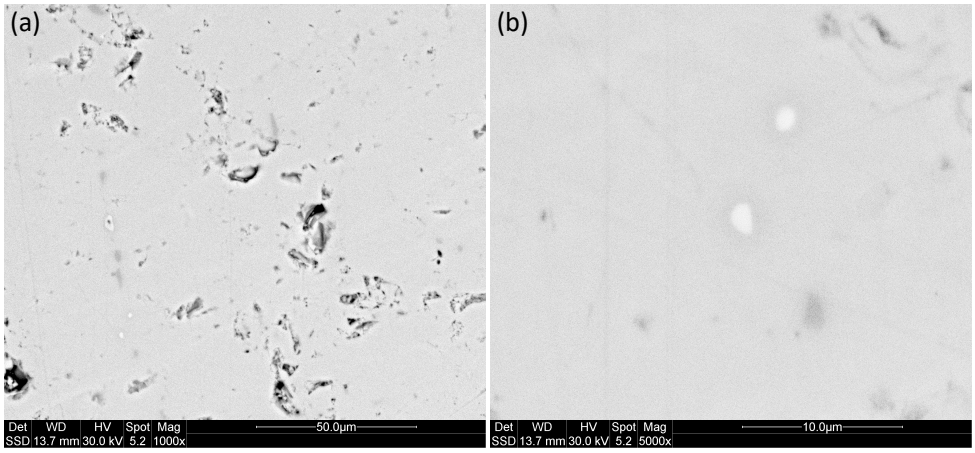

Figure S20 (a) 1000x and (b) 5000x magnification for a nominal stoichiometry of $Ag_{0.98}InTe_2Ge_{0.02}$ showing a matrix of $AgInTe_2$ with approximately 1.5% Ge incorporated. Bright spots are Ge-deficient GeTe with Ag and In incorporated.

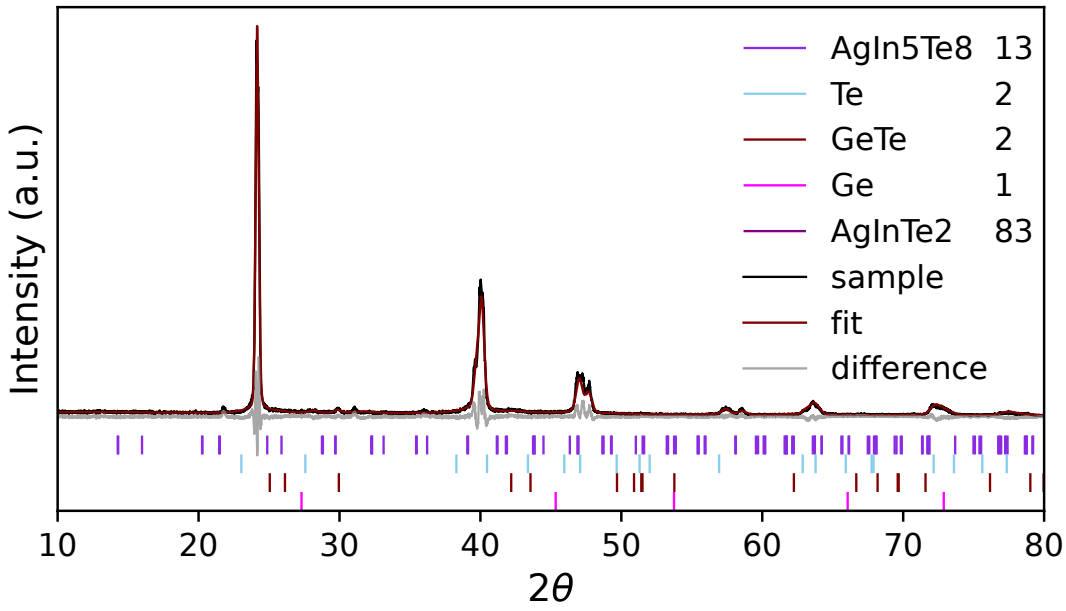

Figure S21 Powder XRD pattern for a nominal stoichiometry of $Ag_{0.98}InTe_2Ge_{0.02}$ largely showing $AgInTe_2$.

2.4 IT2 + Zn

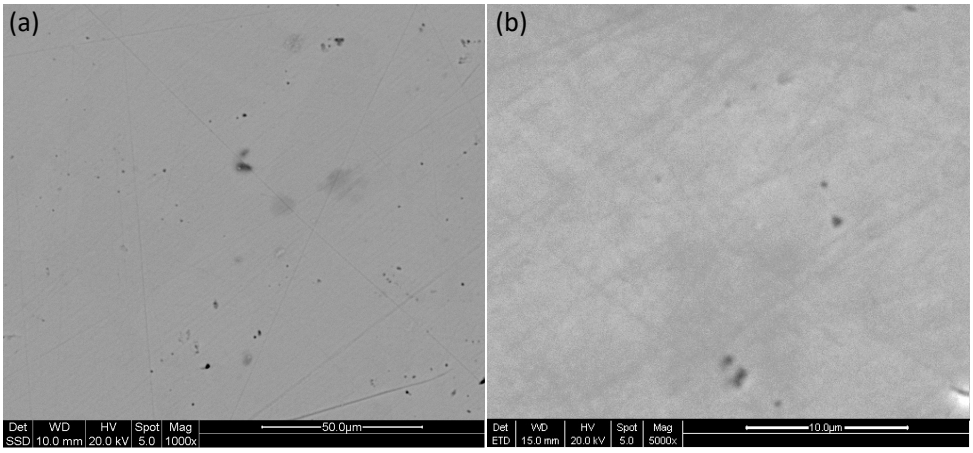

Figure S22 (a) 1000x and (b) 5000x magnification for a nominal stoichiometry of $Ag_{0.98}InTe_2Zn_{0.02}$ showing a matrix of $AgInTe_2$ with approximately 1.5% Zn incorporated.

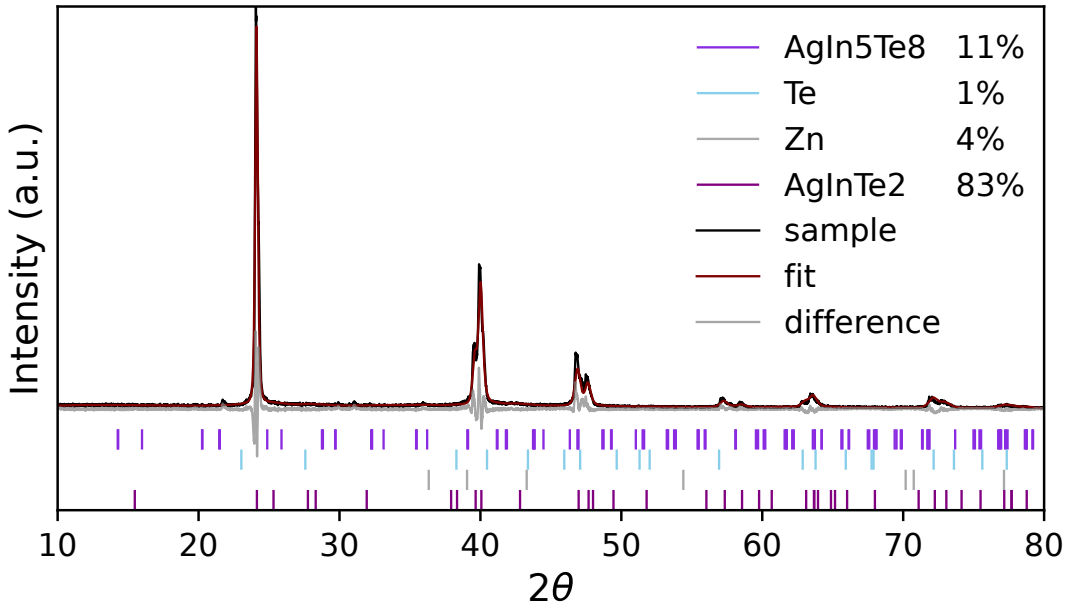

Figure S23 Powder XRD pattern for a nominal stoichiometry of $Ag_{0.98}InTe_2Zn_{0.02}$ largely showing $AgInTe_2$.

3 Defect Diagrams

The defect diagrams for each region of chemical potential space were generated in addition to the Brouwer diagrams shown in the manuscript. For each of the numbered regions of composition space (or points in chemical potential space), the defect diagrams in Figure S24 were computed using the same methods as discussed in the Methods section of the main paper.

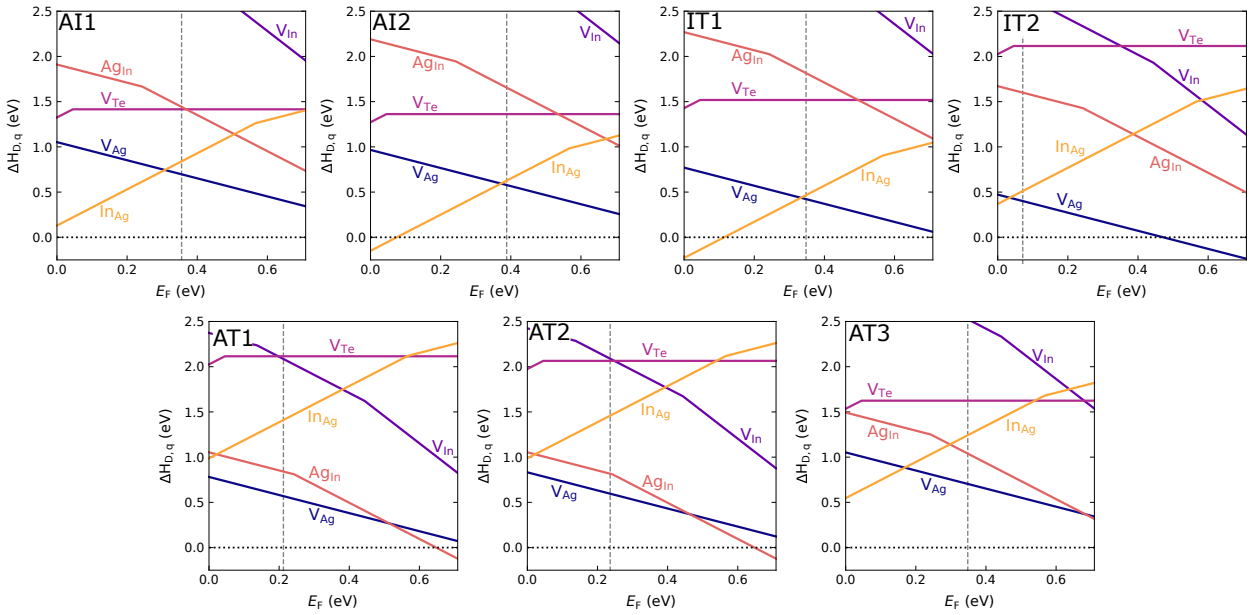

Figure S24 Defect diagrams for each region of chemical potential space. The equilibrium Fermi level is shown by the dotted vertical line.

4 Speed of Sound

Table S1 Experimentally measured speed of sound for samples presented in the main body of this work. Samples were measured at room temperature. Speed of sound was not measurable for sample IT2.

Compound	**Shear SOS (m/s)**	**Longitudinal SOS (m/s)**
AI2	1528	3165
IT2	–	–
AI2 + Ge	1446	2882
IT2 + Ge	1443	2894
AI2 + Zn	1393	2705
IT2 + Zn	1496	3079
Average $CuInTe_2$	1896	3595

5 Equilibrium Fermi Level Positions

Table S2 Equilibrium position of the Fermi level for each point in chemical potential space at 300K and 723K for defect concentrations set by the synthesis temperature of 723K.

Region	**E_F @ 300K (eV)**	**E_F @ 723K (eV)**
AI1	0.11	0.36
AI2	0.13	0.39
IT1	0.11	0.35
IT2	0.0	0.07
AT1	0.05	0.21
AT2	0.06	0.24
AT3	0.11	0.35

6 Equilibrium Chemical Potential Points

Table S3 Equilibrium Fermi level points for each invariant point in equilibrium with $AgInTe_2$. All points are in equilibrium with $AgInTe_2$ and had $AgInTe_2$ experimentally observed, so they are not included in the list of predicted or observed phases for brevity.

Region	$\Delta\mu_{\mathbf{Ag}}$ **(eV)**	$\Delta\mu_{\mathbf{In}}$ **(eV)**	$\Delta\mu_{\mathbf{Te}}$ **(eV)**	Predicted Phases	Observed Phases
AI1	0	-0.278	-0.7	Ag, Ag_9In_4	Ag, Ag_3In
AI2	-0.086	-0.085	-0.753	Ag_9In_4, In_4Te_3	Ag_3In, InTe
IT1	-0.282	-0.202	-0.597	In_4Te_3, $AgIn_5Te_8$	InTe, $AgIn_5Te_8$
IT2	-0.58	-1.097	0	$AgIn_5Te_8$, Te	$AgIn_5Te_8$, Te
AT1	-0.271	-1.406	0	Te, AgTe	Te, AgTe
AT2	-0.22	-1.355	-0.051	AgTe, Ag_2Te	AgTe, Ag_2Te
AT3	0	-0.695	-0.491	Ag_2Te, Ag	Ag_2Te, Ag

7 High Temperature Carrier Concentration

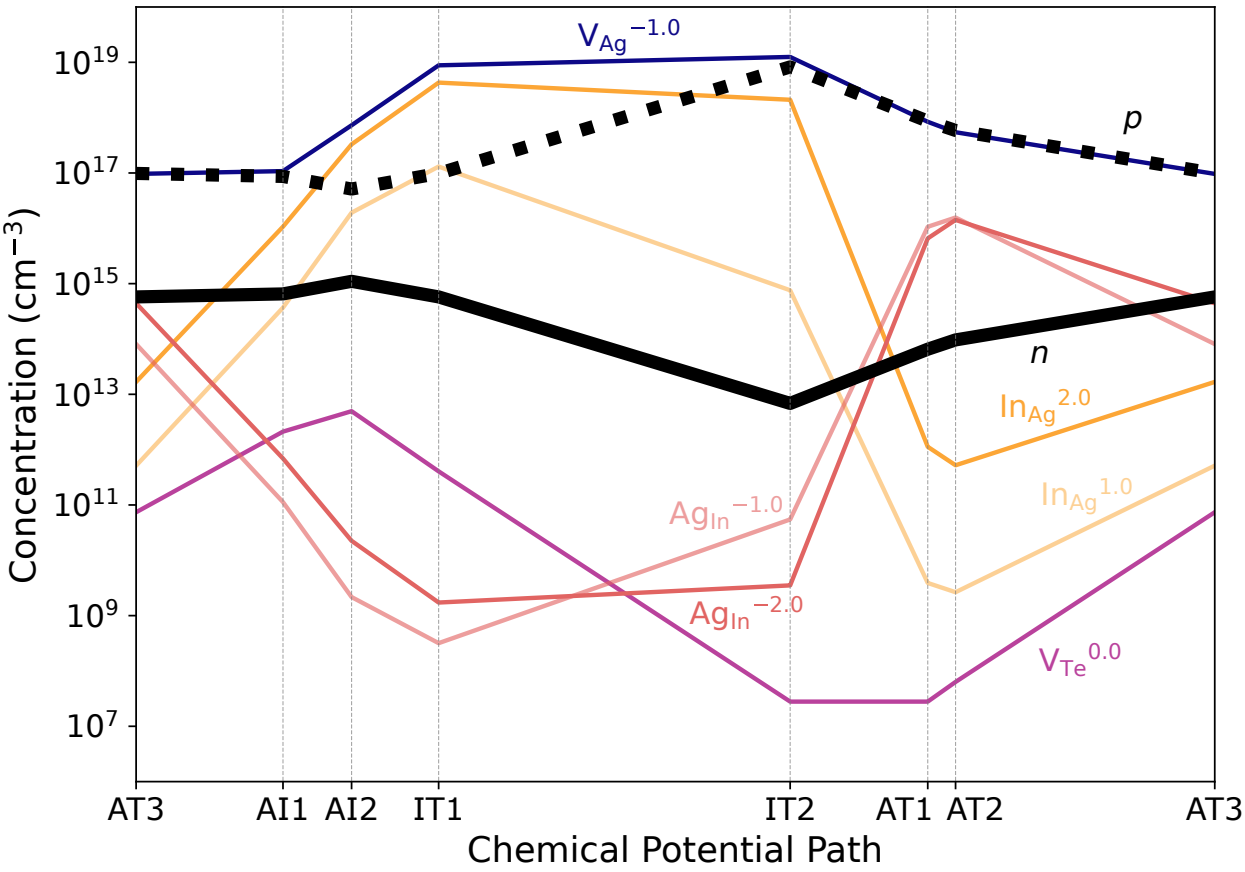

Figure S25 Carrier and defect concentrations through chemical potential space at 723K for defect concentrations set by a synthesis temperature of 723K.

8 AT1: Seebeck and Resistivity

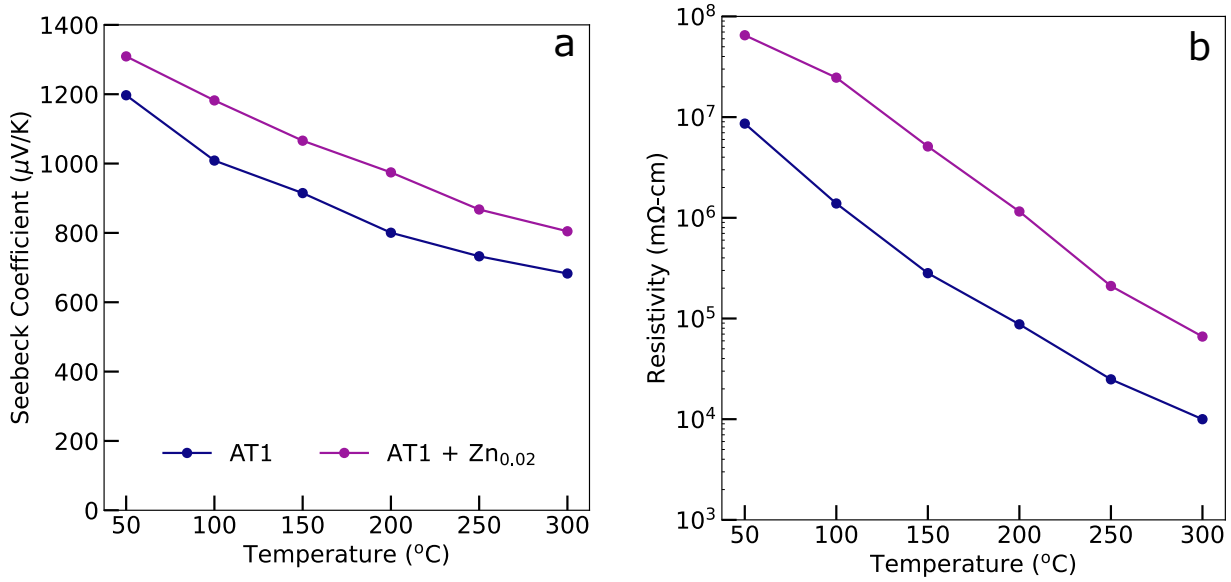

Figure S26 Seebeck and resistivity measurements of samples AT1 and AT1 doped with Zn.